Aochi and Ide *Earth, Planets and Space* (2017) 69:94
DOI 10.1186/s40623-017-0676-5

Earth, Planets and Space

FULL PAPER

Open Access

Role of multiscale heterogeneity in fault slip from quasi-static numerical simulations

Hideo Aochi[1,2,3*] and Satoshi Ide[4]

Abstract

Quasi-static numerical simulations of slip along a fault interface characterized by multiscale heterogeneity (fractal patch model) are carried out under the assumption that the characteristic distance in the slip-dependent frictional law is scale-dependent. We also consider slip-dependent stress accumulation on patches prior to the weakening process. When two patches of different size are superposed, the slip rate of the smaller patch is reduced when the stress is increased on the surrounding large patch. In the case of many patches over a range of scales, the slip rate on the smaller patches becomes significant in terms of both its amplitude and frequency. Peaks in slip rate are controlled by the surrounding larger patches, which may also be responsible for the segmentation of slip sequences. The use of an explicit slip-strengthening-then-weakening frictional behavior highlights that the strengthening process behind small patches weakens their interaction and reduces the peaks in slip rate, while the slip deficit continues to accumulate in the background. Therefore, it may be possible to image the progress of slip deficit at larger scales if the changes in slip activity on small patches are detectable.

Keywords: Multiscale heterogeneity, Fault asperity, Slip-strengthening, Slip-weakening, Seismic cycle, Aseismic slip

Introduction

Slow slip events (SSEs) at various scales have been observed and studied in many regions worldwide over the past two decades (e.g., Linde et al. 1996; Dragert et al. 2001; Obara 2002; Kostoglodov et al. 2003; Ide et al. 2007a, 2008; Ide 2012). It is considered that SSEs occur along the same interface as ordinary tectonic earthquakes (Ide et al. 2007b), generally at the deeper extent of the shallow locked region, below the brittle–ductile transition. Elucidating the mechanics of SSEs is thus important, in terms of both understanding their complex behaviors, such as their spatiotemporal migration and regular recurrence intervals, and also recognizing their potential relationship to large earthquakes, particularly when considering the evolution of frictional strength with sliding (e.g., Shibazaki and Iio 2003; Liu and Rice 2005; Colella et al. 2012).

The dynamic process of earthquake rupture is governed by the energy balance between the released elastic energy and the fracture energy along the interface, with its transient frictional behavior being characterized by a slip-weakening process after the onset of rupture (Ida 1972; Palmer and Rice 1973). This has been proved for many earthquakes through kinematic inversions (Ide and Takeo 1997; Mikumo et al. 2003), forward modeling (Olsen et al. 1997; Aochi and Fukuyama 2002), and dynamic inversions (Peyrat et al. 2004; Di Carli et al. 2010; Ruiz and Madariaga 2011). The most important feature is the scaling relation, which states that fracture energy is proportional to earthquake size (e.g., Ohnaka 2003), regardless of the complexity of the source process. Ide and Aochi (2005) proposed a multiscale heterogeneity concept for earthquakes to uniformly describe the complexity of the earthquake rupture process at any scale. This concept requires that: (1) fault heterogeneity is expressed as the superposition of circular patches of different sizes following a fractal distribution and (2) each patch is attributed fracture energy that is proportional to the patch size. Since stress drop does not change significantly over several magnitudes (e.g., Ide and Beroza

*Correspondence: aochi.hideo@gmail.com
[1] Bureau de Recherche Géologiques et Minières, 3 Avenue Claude Guillemin, BP36009, 45060 Orléans, Cedex, France
Full list of author information is available at the end of the article

Springer Open

© The Author(s) 2017. This article is distributed under the terms of the Creative Commons Attribution 4.0 International License (http://creativecommons.org/licenses/by/4.0/), which permits unrestricted use, distribution, and reproduction in any medium, provided you give appropriate credit to the original author(s) and the source, provide a link to the Creative Commons license, and indicate if changes were made.

2001), condition (2) is represented in terms of the characteristic slip distance of slip-weakening friction with a scale-invariant stress condition (Ide and Aochi 2005). Such frictional scaling can be a universal feature of the interfacial frictional behavior or the fracture medium and can be applied to both single coseismic processes and sequences of the rupture process along an interface (e.g., Ito et al. 2007; Aochi and Ide 2009; Rohmer and Aochi 2015).

This multiscale heterogeneity concept has been successfully applied to the 2011 Mw9.0 Tohoku earthquake to explain its complex rupture behavior (Aochi and Ide 2011; Ide and Aochi 2013, 2014), particularly in identifying how this mega-earthquake had grown from a small initial process. The vast rupture area of this event covered the rupture areas of several past large earthquakes (e.g., a M7.3 foreshock two days before, and the 1978 M7.5 and 2005 M7.0 earthquakes offshore from Miyagi prefecture), as well as a shallower zone that had previously been considered a stable aseismic zone. This new and expansive rupture process indicates that fault heterogeneity is more complicated that what was thought in interpreting the mechanics of mega-earthquakes. Instead of characterizing a mono-scale feature, various asperities of different scales and behaviors are likely to be involved in the fault processes of such mega-earthquakes (Lay et al. 2012; Ide 2014).

Recent numerical simulations of the fault interface have considered this intricate frictional behavior (Noda and Lapusta 2013; Galvez et al. 2014). Both SSEs and standard earthquakes can be mechanically solved in the same framework, where continuum mechanics are coupled with a given friction law and the fault parameters (slip, slip velocity, and/or state of the fault rheology) evolve during seismic cycles. Essentially, the shear stress decreases during an earthquake (weakening process) and increases during the interseismic period (strengthening) of the seismic cycle. The simplified multiscale concept, consisting of a small patch and a large patch, has been applied to the discussion of full seismic cycles under the rate- and state-dependent friction law, with a particular focus on how small heterogeneities can affect the initiation process of a large earthquake (Noda et al. 2013). Some large earthquakes can nucleate from either a dynamic perturbation on a small heterogeneity or a static nucleation process (Ellsworth and Beroza 1995), thus highlighting the importance of the shear stress loading mechanism on the system (Ando et al. 2010). It is also proposed that the many aspects of SSEs and their associated tremors can be modeled by a critical (near-) zero weakening relationship during slip (Ben-Zion 2012; Zigone et al. 2015) or some combination of velocity weakening and strengthening (Ando et al. 2012). One of the aims of this study is to explicitly model the fault healing process after coseismic slip by applying a slip-strengthening/slip-weakening frictional behavior to the system.

Ide (2014) proposed a hierarchical structure over a wide range of heterogeneities, including a characteristic large asperity and small SSE patches, which implies that the upper and lower limits of the hierarchical structure (i.e., the size of the largest and smallest patches) might control the overall behavior of the fault slip. We therefore address, in a general sense, the question of what may happen to the system if the frictional behavior of strengthening and weakening is changed during seismic cycles and how this multiscale concept is applicable, yet different, to both a stable loading system and a stick–slip system (Aochi and Ide 2009). We start with a single patch to explore the scaling relationship in fault slip, and then discuss the interaction between two patches. Finally, we investigate many patches possessing multiscale heterogeneity. Extending from the suggested framework of Ide (2014), this study employs numerical simulations to demonstrate how the occurrence of small events (i.e., the behavior of small patches) changes due to the surrounding large patch or background behavior.

Model and method

Model configuration

Figure 1A shows the model configuration of this study. We prepare a finite model domain for an infinite planar fault Σ_∞ in a 3D infinite elastic medium and assume that the rest of the fault plane is dragged at a constant tectonic speed V_{pl} (i.e., the imposed slip evolves linearly with time: $w_{pl} = V_{pl}t$, where w_{pl} is the steady slip progress of the rest of the fault plane). In the model domain, slip w is expressed as

$$w = w_{pl} + dw, \tag{1}$$

where $(-dw)$ is a differential slip with respect to the steady slip progress of the surrounding part w_{pl} and is often cited as "slip deficit." The shear stress at any point on the fault is written as the spatial convolution over the fault plane Σ_∞:

$$\tau\left(\vec{x}\right) = \int_{\Sigma_\infty} G\left(\vec{x} - \vec{\xi}\right) \cdot \left(w_{pl} + dw\left(\vec{\xi}\right)\right) \mathrm{d}\Sigma_\infty, \tag{2}$$

where G is a response function of the medium (Green's function). In this study, we assume the fault plane is embedded in a homogeneous, infinite elastic medium, such that the discrete forms of G are analytically defined (Tada et al. 2000). The contribution of w_{pl} over the whole infinite fault plane is zero, indicating a rigid body movement. Thus, Eq. (2) can be rewritten with only the slip-deficit $(-dw)$ component on the modeled area Σ:

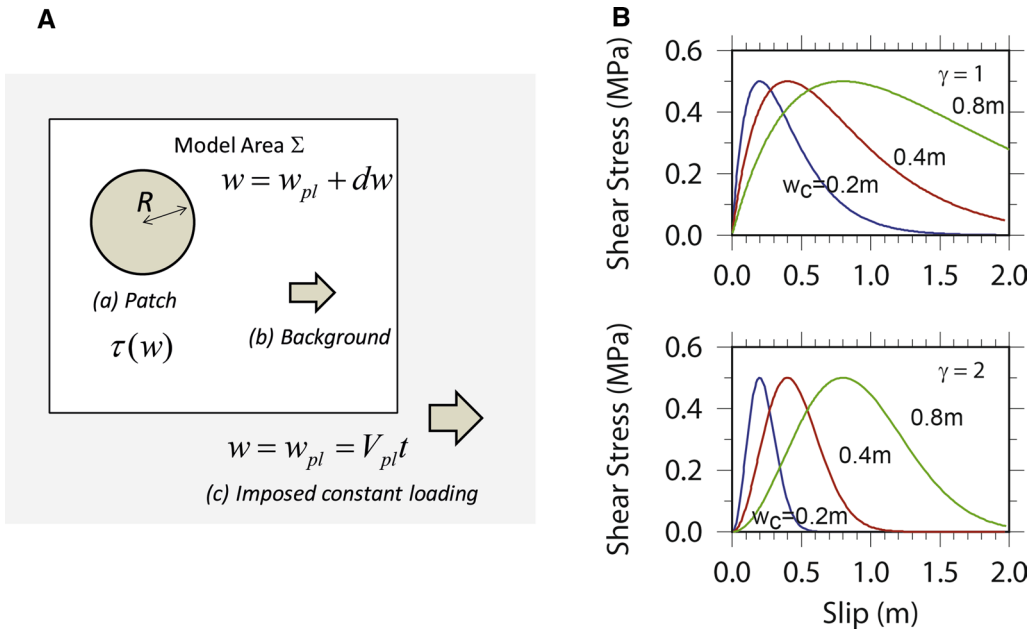

Fig. 1 **A** Schematic illustration of the model configuration for a single patch surrounded by aseismic slip. The model area is described by: *a* a patch with radius *R*, governed by a friction law that is dependent on the parameters of the patch; *b* the background, which may possess a zero-friction condition or simply be the largest patch existing behind *a*; and *c* a constant loading outside of the model area. The infinite domain Σ_∞ from Eq. (2) consists of *a* to *c*, while the modeled area is limited to *a* and *b*. **B** Examples of frictional behavior, from Eq. (4), with $\gamma = 1, 2$ and $w_c = 0.2, 0.4,$ and 0.8 m. In this case, $\Delta\tau = 0.5$ MPa and $w_0 = 0$ m

$$\tau(\vec{x}) = \int_{\Sigma} G\left(\vec{x} - \vec{\xi}\right) \cdot \mathrm{d}w\left(\vec{\xi}\right) \mathrm{d}\Sigma, \tag{3}$$

which simplifies the analysis. This stress can then be equilibrated with any given friction relation for τ (as demonstrated in the following section).

Fractal patch model with a slip-strengthening process

We extend the fractal patch model previously developed for explaining the coseismic phase of earthquake dynamics (Aochi and Ide 2004, 2009; Ide and Aochi 2005) by allowing aseismic slip prior to the slip-weakening process. If we take the 2011 M9 Tohoku earthquake, Japan, for which the average coseismic slip was ~20 m (maximum of ~60 m), the accumulated slip deficit is ~100 m (assuming 0.1 m/yr and a recurrence time of 1000 years). Some limited areas of the interface are recognized as slip-deficit zones (strong seismic coupling), such as the Miyagi-oki ~M7.5 earthquakes (recurring every ~40 years; e.g., Hashimoto et al. 2009). However, it is considered that most part of the fault surface was aseismically sliding, thus contributing to the stress release associated with the 2011 earthquake. To capture these heterogeneities, we introduce a slip-dependent friction law to our model that varies gradually from strengthening to weakening behavior. This transition is observed in laboratory experiments shortly before slip-weakening (e.g., Ohnaka 2003; Brantut and Viesca 2015) and has been implemented in previous numerical modeling studies (Ohnaka and Yamashita 1989; Shibazaki and Matsu'ura 1995). In most numerical modeling of the coseismic earthquake process, this strengthening process is neglected, because the contribution from the strengthening phase to fracture energy release is considered minor once the instability develops. However, we aim to model much longer strengthening processes that correspond to the long-term healing process after the previous weakening process during a seismic cycle (e.g., Nakatani, 2001; Aochi and Matsu'ura 2002). By extending the slip-dependent law used by Shibazaki and Matsu'ura (1995), we describe friction as an evolution of the shear stress τ:

$$\tau = f(w) = \begin{cases} \Delta\tau \left(\frac{w-w_0}{w_c}\right)^{\gamma} \exp\left(1 - \left(\frac{w-w_0}{w_c}\right)^{\gamma}\right) & \text{for } w \geq w_0 \\ 0 & \text{for } w < w_0 \end{cases}, \tag{4}$$

where $\Delta\tau$ is the strength drop (peak strength, assuming zero residual stress), $\gamma > 0$, and w_c and w_0 are constants. As illustrated in Fig. 1B, w_c characterizes the amount of slip (or distance) until the peak strength is achieved (as well as the following weakening process), and the

shape parameter γ defines the curve of frictional behavior. Ohnaka (2003) found a linear scaling relationship between the distances of the strengthening and weakening processes, demonstrating that this one-parameter description is a good approximation. We thus define w_c as the characteristic distance and w_0 as the phase shift. Equation (4) has a peak at $w = w_0 + w_c$. Shibazaki and Matsu'ura (1995) explored the nucleation process of earthquakes for $\gamma = 1$ and $w_0 = 0$; we extend their study and also consider the cases where $\gamma \neq 1$ and $w_0 \neq 0$. When $\gamma > 1$, τ remains low for longer durations and then increases quickly [as the derivative of Eq. (4) is zero at $w = w_0$], corresponding to a fast healing process arriving just prior to weakening process.

Fault heterogeneity is generally described by patches of different sizes (Ide and Aochi 2005; Aochi and Ide 2009). For each patch, we assign a particular frictional parameter (w_c) based on the size of the patch, but we keep the same value of $\Delta\tau$ on all patches to sustain the broad scaling relationship for stress drop (e.g., Kanamori and Anderson 1975; Ide and Beroza 2001). According to Ide and Aochi (2005), w_c is proportional to the patch size R, such that

$$w_c \propto R. \tag{5}$$

This assumption highlights the fact that earthquakes are generally scale-independent processes from the viewpoint of earthquake seismology. Ohnaka (2003) summarized the scaling relationship from laboratory-scale studies to large earthquakes. Uchide and Ide (2010) analyzed earthquakes over a wide range of magnitudes to statistically show that rupture growth is self-similar. We then assume that the same scaling relationship is applicable both to the dynamic, coseismic process of earthquakes (slip-weakening friction) and to the preparation process (slip-strengthening friction).

Numerical method and parameters

Equations (3) and (4) are solved simultaneously for the two unknowns τ and dw over the model area Σ, such that the loaded shear stress due to the slip distribution is balanced by the frictional behavior of the system. We discretize the fault plane as a series of small square elements of size Δs that experience uniform slip (dw) at a given time step. We can then write the shear stress τ_i for the ith element in the discrete form

$$\tau_i = \sum_n G_{\mathrm{in}} \cdot dw_n = f\left(w_{pl} + dw_i\right), \tag{6}$$

where G_{in} is a response function from the nth to ith element. Note that τ_i is influenced by not only the ith element but also all other elements ($n \neq i$). We adapted the Levenberg–Marquardt method to solve Eq. (6) iteratively (e.g., Press et al. 1992). Note that the solution $dw_i = 0$ is only valid when, independent of our slip calculation, the friction is modeled as constant. The physical quantities of the key parameters that define our model space are summarized in Table 1. Large patches are defined as a few tens of kilometers in size, based on significant aseismic phenomena observed in some subduction zones (e.g., Ide et al. 2007a, b). We note that our fixed $\Delta\tau$ may be smaller than that inferred for standard earthquakes. For example, Gao et al. (2012) infer a range between 0.01 and 1 MPa from SSEs in Cascadia, and Maury et al. (2014) infer a value of ~0.1 MPa from the large 2010 SSE in Guerrero, Mexico. We fix a value of $\Delta\tau = 0.5$ MPa for our study. We further note that the stress accumulation is not led by the stress increment but by the slip deficit. While our study focuses on a fault interface, the following results and discussions can be downscaled to local microseismicity or laboratory experiments. At time $t = 0$, we set $w_{pl} = 0$, $dw = 0$, and $\tau = 0$ everywhere, and w_{pl} increases at a constant rate (via the loading rate v_{pl}) for each time step. As there is no time dependency in Eqs. (3) and (4), the time step can be viewed as a slip step imposed outside the model area. Therefore, the system described here is relative in its stress level and in time, and can be extrapolated to other scales.

Parameter studies

In this section, we study the characteristics of the introduced slip-dependent law, with an emphasis on the role of the slip-strengthening process. We focus on the scaling issue to address how the stress (slip deficit) is accumulated prior to the slip-weakening process, according to the size of a single patch (Scale dependency in the accumulation process (scaling in w_c) section), and then explore the behavior of a small patch surrounded by a large patch (Incoherent onset of stress accumulation (variation in w_0) section). An understanding of both features is important in explaining the consequent weakening process.

Scale dependency in the accumulation process (scaling in w_c)

We first explore the behavior of a single patch of varying size (different w_c). According to Eq. (4), the peak

Table 1 Model parameters

Parameter	Quantity
Medium rigidity μ	50 GPa
Grid size Δs	4 km, 2 km, 1.5 km
Strength drop $\Delta\tau$	0.5 MPa
Increment of tectonic loading w_{pl}	0.01 m
Loading rate v_{pl} /Time step Δt	0.01 m/Δt
First patch level (size R, characteristic distance w_c)	40 km, 80 cm

strength $\tau = \Delta\tau$ at the turning point from the strengthening to the weakening process does not vary with patch size. However, the stress accumulation is more rapid on a smaller patch than on a larger patch under the same background loading rate. As shown in Fig. 1A, we set a single patch in the model domain and employ the model parameters summarized in Tables 1 and 2. We then vary the patch radius and the scaling relation of w_c in Eq. (4). Figure 1B illustrates the frictional relationship, assuming w_c scales with respect to R. Here, $w_c = 0.2, 0.4$, and 0.8 m correspond to $R = 10, 20$, and 40 km, respectively.

Figure 2a and b provides a snapshot of a single patch with radius $R = 20$ km, $w_0 = 0$, and $\gamma = 2$. The slip deficit initially increases with time, leading to stress accumulation. The patch then slips to catch up with the surrounding region, releasing the accumulated stress after the peak friction is reached in Eq. (4). We study the effect of different values of γ and R on slip deficit, listed in Table 2, where w_c is scale-dependent. The stress and slip evolutions are qualitatively similar in all cases. Here we are interested in how the slip-deficit phenomena are scaled. As shown in Fig. 2c, the time necessary to achieve the peak slip deficit is proportionally scaled with R and independent of γ; a similar trend is observed in the amount of peak slip deficit (Fig. 2d). Note that if there is no scale dependency on w_c, the time to the peak slip deficit scales differently for different values of γ and R (pale gray small circles and line in Fig. 2c, where $w_c = 0.4$ m). Therefore, one can conclude that the time to the peak slip deficit is only scale-invariant according to the scale dependence of w_c. On the other hand, the amount of peak slip deficit is dependent on the geometrical size of the patch and is independent of its frictional parameters.

Figure 3 shows the evolution of the slip deficit and the average slip rate for each patch to quantify the scaling relationship for different values of γ ($\gamma = 1$ and 2), assuming that w_c is scale-dependent (see Fig. 1B). The weakening process after the peak stress is reached accelerates the fault slip (i.e., reduces the slip deficit). Figure 3a shows that in the case where $\gamma = 1$, the increasing rate of the slip deficit with time is common for all cases, such that the initial slip rate at $t = 0$ is invariant from R. However, the amplitude of the slip rate is inversely related to R if $\gamma = 2$ (Fig. 3a). The stress (slip deficit) is accumulated and released faster on a smaller patch than on a larger patch. This is a generality for cases where $\gamma > 1$.

From these preliminary tests, we find that the behavior of this system for the case where $\gamma = 1$ is characterized by universal functions, which can be normalized over time according to the scale. Such scaling is known for the nucleation and the dynamic process of earthquakes (Aochi and Ide 2004 and references therein), which is important for understanding both the loading and weakening processes of aseismic slip. This is based on the fact that the elastic equation for a fault (Eq. 6) is governed by a non-dimensional rigidity, $L_c = (\mu/\Delta\tau) \cdot (w_c/R)$ (Matsu'ura et al. 1992), with medium rigidity μ. In the case that the frictional evolution is scale-dependent (as in Eq. 5), it is expected that slip behaviors appear as scale-independent. Since the slip rate is controlled by a factor of $R \times$ (maximum slope of friction law), one expects that the slip rate is scale-independent if $\gamma = 1$ in Eq. (4). However, for cases where $\gamma > 1$, this scale invariance is not applicable, as a smaller patch has a sharper and higher slip rate function than a large patch. This scale dependency might be consistent with slow earthquake observations where only small slow earthquakes (tremors) are detected. The particularity of Eq. (4) is that $\frac{d\tau}{dw}\Big|_{w=0} \neq 0$ if $\gamma = 1$, while $\frac{d\tau}{dw}\Big|_{w=0} = 0$ for $\gamma \geq 1$. This means that the evolution of the slip deficit at $w = w_0$ is discontinuous for $\gamma = 1$; the slope of the slip-deficit function ($dw \neq 0$ on the patch) shows a sudden change at $t = 0$, while it changes gradually ($dw \sim 0$ on the patch) in the latter case.

Table 2 Variables for a single patch case

Parameter	Quantity
Patch size R	40, 20, 10, and 5 km
Characteristic distance w_c	Proportional to R
Shape parameter γ	1, 1.1, 1.5, 2, and 3
Phase factor w_0	0 (fixed)

Incoherent onset of stress accumulation (variation in w_0)

We now consider two patches of different sizes superposed along the fault surface. Their frictional parameter distributions are shown in Fig. 4. A large patch (L) of radius $R = 40$ km and a small patch (S) of radius $R = 10$ km are modeled, with the model parameters summarized in Table 3. The frictional characteristics of the smaller patches appear locally if different patches are superposed. We aim to show how the behavior of a small patch is affected by the friction of the surrounding large patch. The small patch has minimal influence on the large patch behavior in this given situation, while smaller patch(es) may impact the occurrence of the large patch quasi-statically (e.g., Noda et al. 2013) or dynamically (Aochi and Ide 2009). As $\Delta\tau$ is the same for both patches, the different attributes of w_c and w_0 vary the behavior of each patch. Here we focus on the role of w_0, setting $\gamma = 2$ to avoid the discontinuous evolution of slip deficit at $w = w_0$, such that $dw = 0$. The initial condition is uniform everywhere ($w = 0$ and $\tau = 0$).

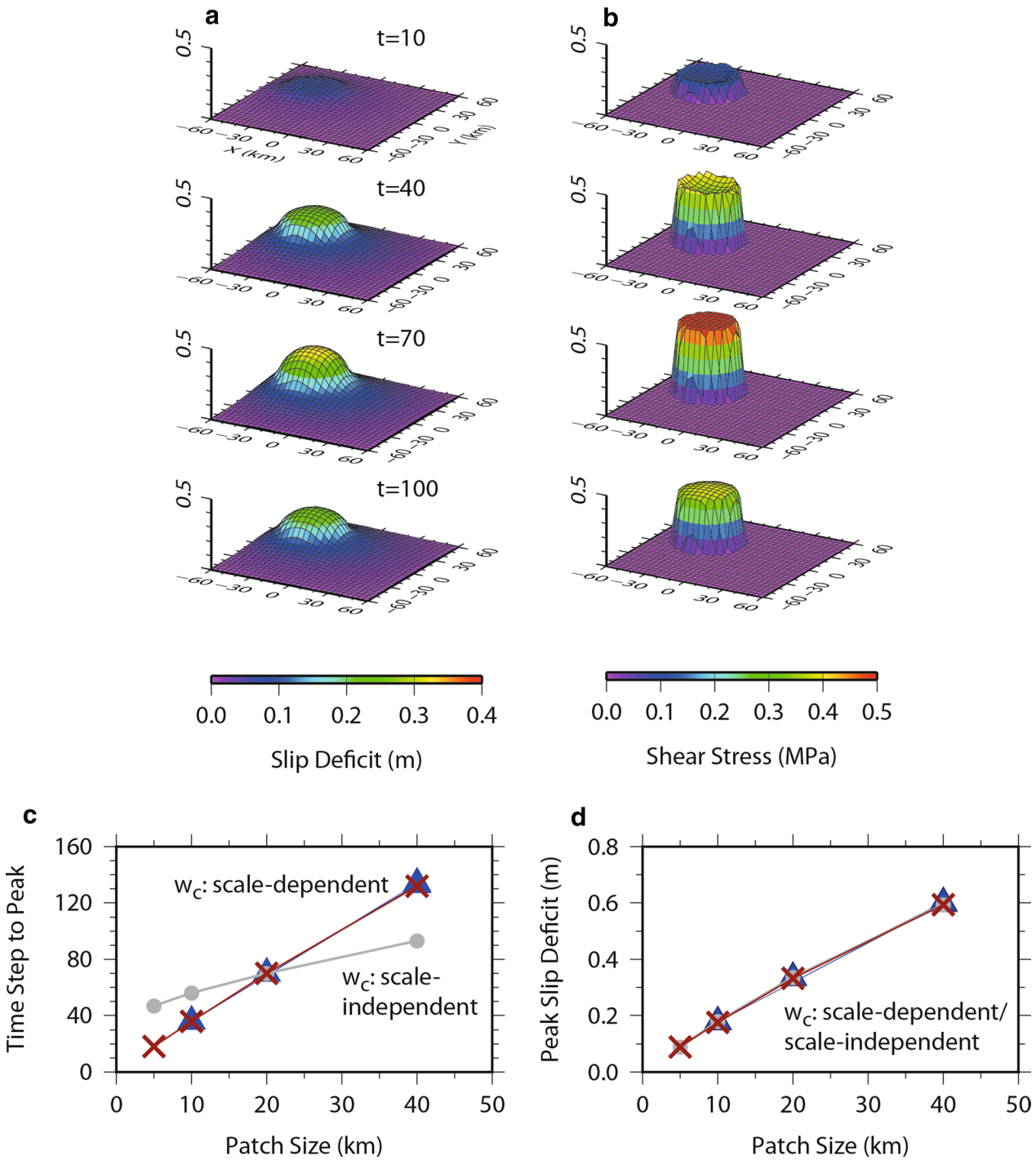

Fig. 2 Snapshot of the quasi-static evolution of fault slip for a single patch of $R = 20$ km, $w_c = 0.4$ m, $w_0 = 0$ m, and $\gamma = 2$, in terms of **a** slip deficit and **b** shear stress. At approximately time step 70, the peak in slip deficit is observed. **c** Time step necessary to reach the peak in slip deficit, with variable R and γ (Table 2). All the cases ($\gamma = 1$, 1.1, 1.5, and 2) are superposed, represented by solid large symbols (*crosses*: $\gamma = 2$; *triangles*: $\gamma = 1$, 1.1, and 1.5) and *lines*. The *pale gray small circles* and *lines* represent the cases where w_c is not scaled with patch size R ($w_c = 0.4$ m fixed). The *small pale gray circles* and *lines* represent the cases where w_c is not scaled with patch size R ($w_c = 0.4$ m fixed). **d** Peak slip deficit at the center of the patch for each case. *Markers* are the same as in the previous panel

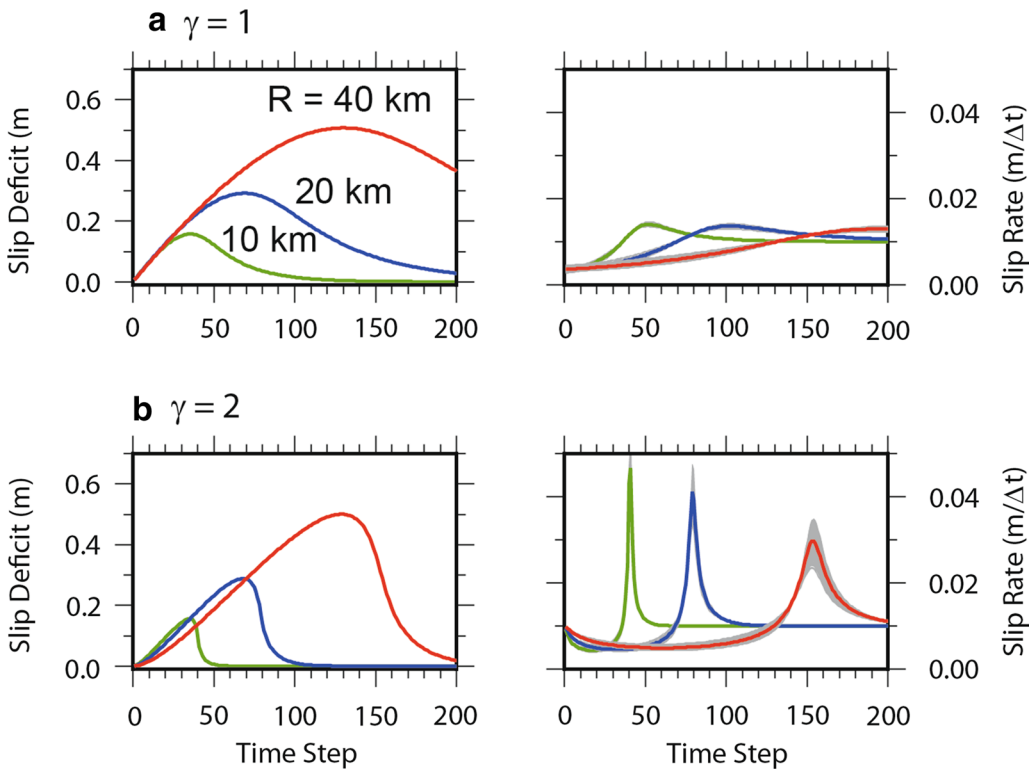

Fig. 3 Evolution of slip behavior in terms of slip deficit and slip rate, averaged for each patch (*center* and *right panels*), for **a** $\gamma = 1$ and **b** $\gamma = 2$. The *three lines* correspond to $R = 10$ (*green*), 20 (*blue*), and 40 (*red*), respectively. In the *right-hand panels*, *gray lines* represent the behaviors of different parts of a patch, and the *solid colored lines* give the average behavior for an entire patch

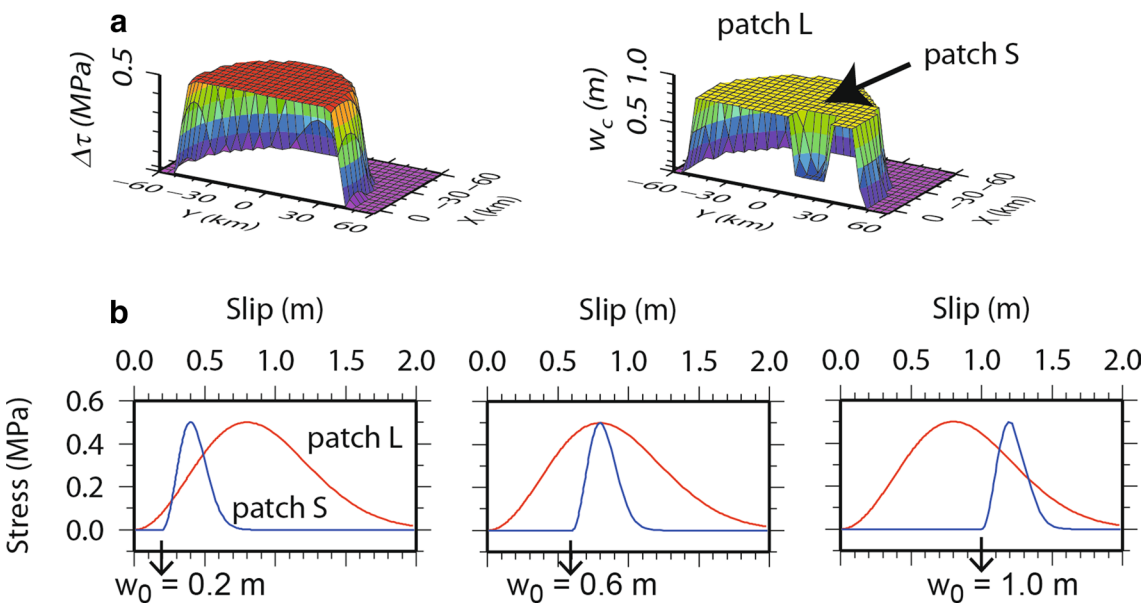

Fig. 4 Model with two patches (L: large; S: small). **a** Distribution of two patches in terms of peak strength $\Delta\tau$ and characteristic distance w_c. The cross section is taken at $x = 5$ km, running through the center of the small patch. **b** Frictional behavior, from Eq. (4), for both L and S, with $w_0 = 0.2, 0.6,$ and 1.0 m

Table 3 Variables for the two-patch case

Parameter	Quantity
Patch size R of large and small patches	40 km (L) and 10 km (S)
Characteristic distance w_c	Proportional to R
Shape parameter γ	2 (fixed)
Phase factor w_0	0 m (fixed) for L 0.2, 0.6, and 1.0 m for S

The simulation results shown in Fig. 5 represent different w_0 values for the small patch, such that there are different positions of the frictional peak ($w_0 + w_c$) on S with respect to just one (w_c) on L. The two time steps (T_1 and T_2) for each sequence are selected when the shear stress has a peak accumulation on either of the two patches. For the first two cases, where $w_0 = 0.2$ m (Fig. 5a) and $w_0 = 0.6$ m (Fig. 5b), S is the first to reach the peak stress and slide, while L does not begin to slide before S until $w_0 = 1.0$ m (Fig. 5c). In all cases, S does not have a significant influence on the aseismic process of L, as the time step of the maximum shear stress accumulation does not change.

Figure 5 also illustrates the detailed evolution of stress at the center of the two patches (S and L), as well as the average slip behavior on each patch. The time taken to reach the peak slip deficit on S changes with w_0. In the first case where $w_0 = 0.2$ m (Fig. 5a), the slip deficit on S is charged and released prior to the peak on L. S also experiences simultaneous and passive slip again when L releases its stress. In the latter cases, where $w_0 = 0.6$ m (Fig. 5b) and $w_0 = 1.0$ m (Fig. 5c), S reaches its peak shear stress when L is already charged or releasing its stress. The slip rate on S becomes much smaller when $w_0 = 0.2$ m (Fig. 5a) compared with larger w_0 values (Fig. 5b, c). This means that the slip behavior of S is overprinted by L, even though the shape of the frictional behavior is the same. It is thus interpreted that the difference arises from the deformation state surrounding S, namely the practical stiffness of the system at each moment. Comparing these results with the coseismic process, it is expected that small patches may keep a high slip rate if rupture onset on them is delayed. Note that the small patches are mostly hidden when a surrounding patch is sliding, if the phase of the peak friction is simultaneous among the patches (e.g., Aochi and Ide 2014).

Multiscale patch models applied to seismic cycles

Here we numerically study the aseismic slip behavior in a multiscale patch model by changing the geometry of patch distributions and the limit of the hierarchical structure. It is expected that the system behavior depends on the spatial distribution of patches even if the same fractal size–number distribution is applied. We focus our discussion by simplifying the model setting and carrying out 15 simulations. We consider three ranks ($k = 2, 3, 4$) of different patch sizes from $R = 20$ to 5 km along a 60 km × 60 km fault surface (one-quarter the size of the previous simulation), such that the background corresponds to the characteristics of the larger patch ($k = 1$). According to Ide and Aochi (2005) and Aochi and Ide (2009), the number of patches at each rank follows a fractal relationship:

$$N_k = 2^{2(k-1)}, \tag{7}$$

and w_c is proportional to R.

Figure 6 illustrates our 15 examples of the randomly generated patch distribution, where an average of 1, 4, and 16 patches are present for ranks $k = 2, 3,$ and 4, respectively. A few patches of the largest rank are sometimes found, but their total area is statistically equivalent to that of one patch. For $k = 2, 3,$ and 4, $w_c = 0.4, 0.2,$ and 0.1 m, respectively, and it is assumed that the frictional behavior of each patch has a cycle of $3 \times w_c$ to represent the fault healing process and then the seismic cycle. This cyclic period is long enough that the shear stress is reduced to approximately zero across each patch. Extending this cyclic period leads to a quasi-zero-stress state that lasts longer, resulting in a longer seismic cycle with weaker coupling on average. This suggests that the fault is always sliding and that the slip amount from a large event (seismic or aseismic) may only form a portion of the total slip. The condition where $w_c = 0.2$ m for a patch of $R = 10$ km (cycle of 0.6 m) leads to a slip event of ~M6, with a potential recurrence interval of several tens of years if the tectonic convergence speed is fast enough. We assume $\gamma = 2$ in Eq. (4) (see Fig. 1B) so that the frictional behavior is quasi-zero during most of interseismic period. The onset distance w_0 is randomly defined. For the background fault interface, we define $w_c = 0.8$ m and $w_0 = 2.4$ m, allowing us to analyze the slip behavior for different background states, namely the zero-stress condition, stress accumulation, and stress releasing phases. As the slip rate is set at 0.01 m per time step, each phase briefly corresponds to the time until step 240, 320, and 400, respectively.

Figure 7 shows the temporal evolution of stress, slip deficit, and slip rate for two cases (4 and 6) from Fig. 6, representing the minimum (4) and maximum (6) background areas among the 15 examples. Shear stress is plotted at the center of each patch, noting that a large patch is sometimes occupied by another small patch. Slip deficit and slip rate are averaged across each patch. After stabilization during the initial 50 time steps, the system behavior becomes quite active, with increases in both the frequency and maximum value of the slip rate. Pink curves represent the

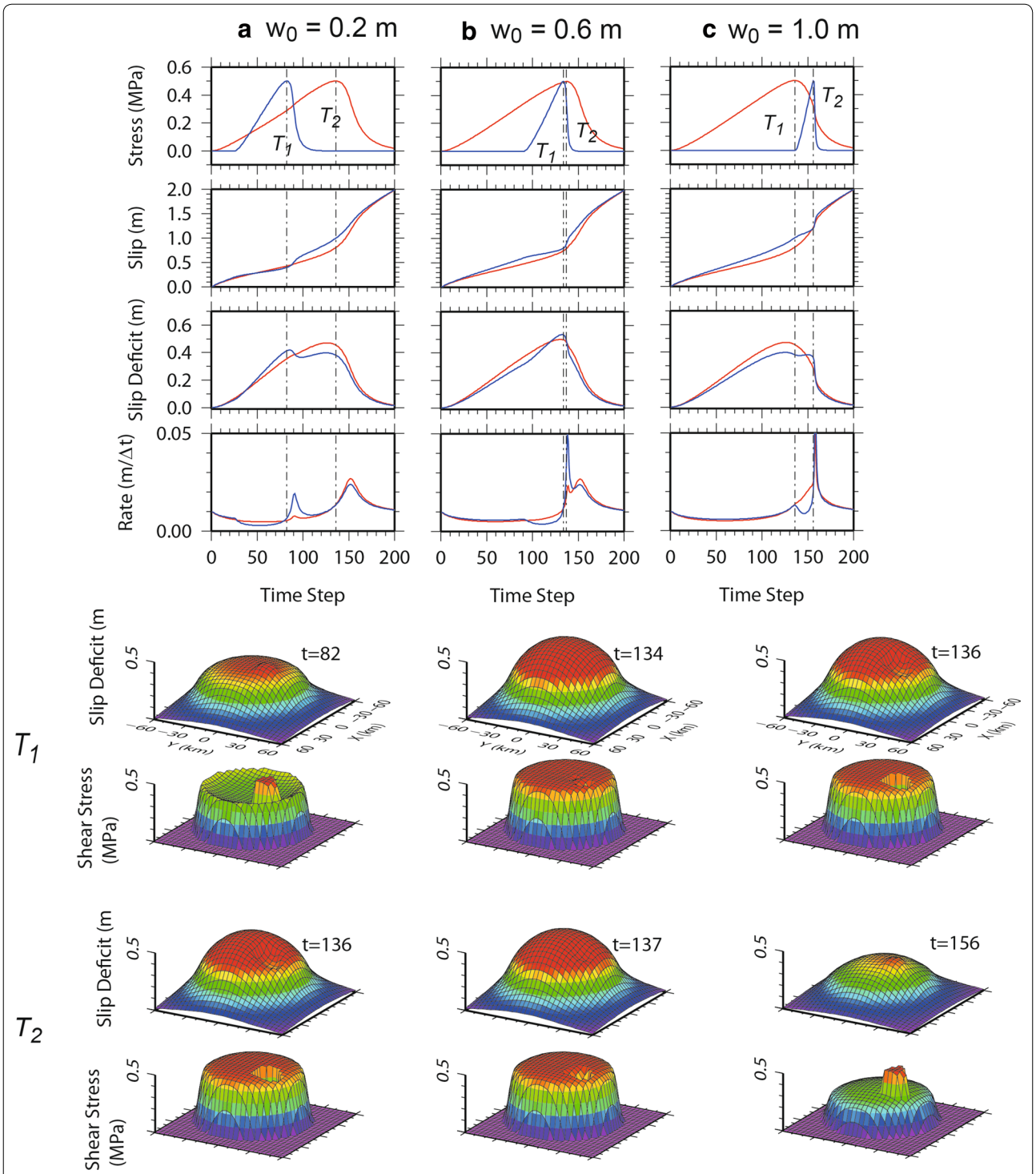

Fig. 5 Evolution of shear stress and slip behaviors for L (*red*) and S (*blue*), where **a** $w_0 = 0.2$ m, **b** $w_0 = 0.6$ m, and **c** $w_0 = 1.0$ m. Plots of temporal changes in shear stress, total slip, slip deficit, and slip rate are shown for each case. Stress values are extracted from the center of each patch, while the slip quantities are averaged across each patch. The times T_1 and T_2 are indicated by *broken lines* when the shear stress has a peak at either of two patches (L or S) just before the weakening process, and the corresponding spatial distributions of slip deficit and shear stress are illustrated in the following figures

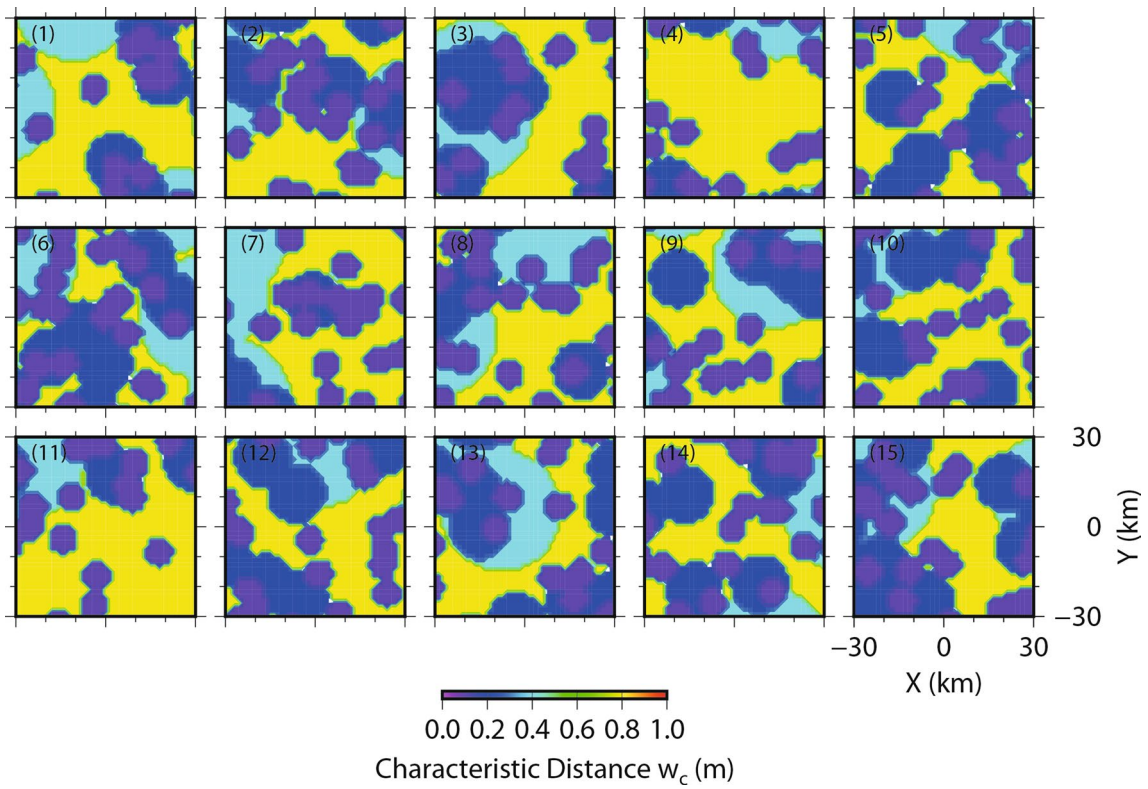

Fig. 6 Spatial distribution of randomly generated multiscale patches for 15 cases, randomly generated under the same fractal size–number distribution. Each model includes three different ranks of patches ($k = 2, 3,$ and 4), denoted by *light blue*, *dark blue*, and *purple*, respectively. The background region is *yellow*, with $w_c = 0.8$m and $w_0 = 2.4$m, and is assumed to represent a larger patch of rank $k = 1$

seismic moment release M_0 (Fig. 7b) and seismic moment release rate along the entire fault plane $\dot{M}_0$ (Fig. 7c), while red points show the local maximum (estimated from the sign change of the derivative) in slip rate for each time step (Fig. 7c). Although the two extreme cases are different in terms of small-scale interactions between patches, closer inspection of the peaks in slip rate indicates that fault rupture due to these patches may be seismologically detectable and that $\dot{M}_0$ may be geodetically detectable in both instances (Fig. 7c). The peaks in slip rate become less frequent in case (4) between time steps 250 and 350 (Fig. 7c), corresponding to the stress accumulation phase of the slip-deficit curve (Fig. 7b). All 15 simulations are summarized in Fig. 8, in terms of both the locally observed maximum slip rate and $\dot{M}_0$ as a function of time. Less frequent peaks in slip rate between time steps 250 and 350 are observed across all simulations (Fig. 8). A distinct and consistent relationship between the locally observed maximum slip rate and $\dot{M}_0$ is also observed, with some variations in amplitude arising due to the specifics regarding patch distribution and interaction.

Moving averages of the number of peaks in slip rate and the maximum slip rate are determined for all 15 simulations to further quantify the temporal variation in slip rate (Figs. 9, 10). A clear reduction in activity between 250 and 350 time steps is evident in both the overall behavior and the local patch slip (Fig. 9). This reduction is also observed in both $\dot{M}_0$ (Fig. 10a) and the observed minimum peak slip rate at about time step 300 (Fig. 10b). Therefore, slip on small patches occurs more frequently and at a faster rate when the background stress is decreasing. However, when the background stress is increasing, the short-term activity evident as peaks in slip rate becomes even weaker than at the other period of the seismic cycle. This observation might be unexpected because we often expect enhanced seismic activity in the case of high stress or rapid stress buildup in the system, but it is in agreement with the simulation using only two patches (Fig. 5), where the slip rate is enhanced during stress release in the background region. This observation is therefore important when interpreting SSEs in nature.

Discussion

We assume that the characteristic distance w_c is proportional to patch size R and randomly define the onset

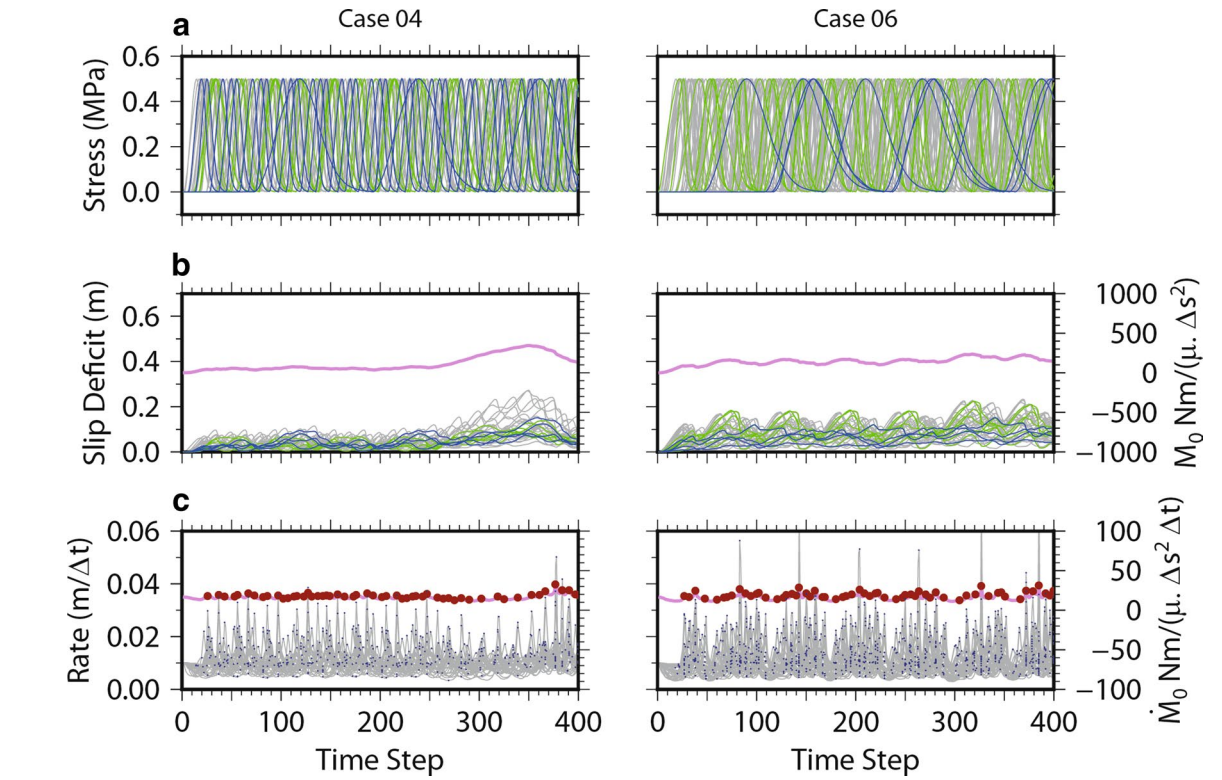

Fig. 7 Simulated temporal evolution for cases (4) and (6), whose patch distributions are shown in Fig. 6. **a** Shear stress evolution at the center of each patch. The *colors* correspond to the order of the patches, with *blue*, *green*, and *gray* used for $k = 2, 3$, and 4, respectively. **b** Average slip deficit across each patch. M_0 is shown by a pink curve. **c** Average slip rate across each patch. $\dot{M}_0$ is shown with a *pink curve*. The local peaks in slip rate are identified by *blue dots*, whereas the *red circles* correspond to the peaks in $\dot{M}_0$ for each time step

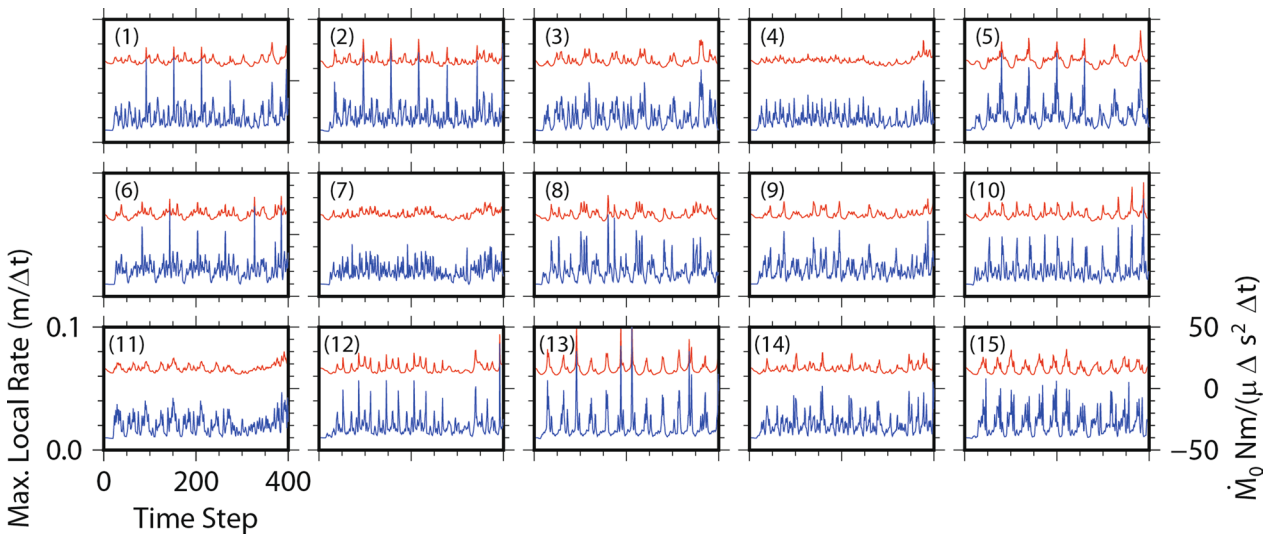

Fig. 8 Temporal evolution of all 15 simulations. The maximum slip rate at each time step is stated in *blue* (*left axis*), and $\dot{M}_0$ from the whole area is in *red* (*right axis*)

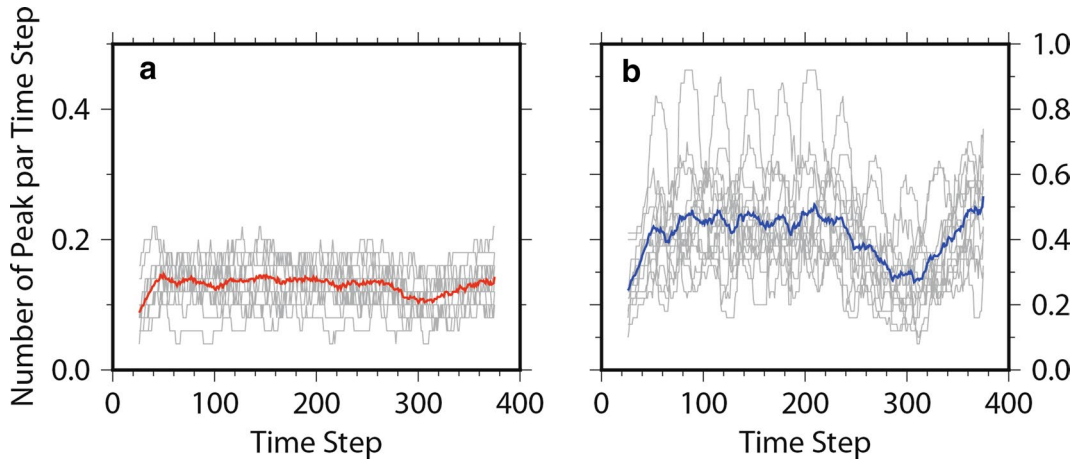

Fig. 9 Number of peaks per time step, averaged over 50 time steps, from the 15 simulations. In **a** and **b**, peaks in $\dot{M}_0$ (corresponding to the *red points* in Fig. 7) and in the local slip rate (*blue points* in Fig. 7, selected for a peak rate higher than 0.02 m/Δt) are shown, respectively, as a function of time step. The *bold colored curves* are the average values for all the simulations

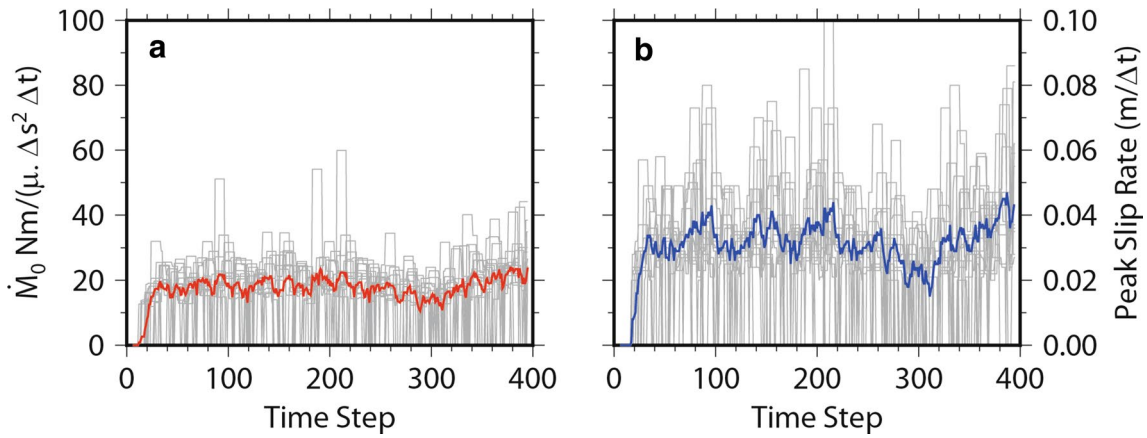

Fig. 10 Peak values of slip rate, averaged over 20 time steps, from the 15 simulations. The overall behavior and local movement are shown in the *left* and *right panels*, respectively. The averages of all the simulations are shown by *bold curves*

distance w_0 to demonstrate the influence of patches on slip along the fault interface. Here we use cases (4) and (6), and employ the same parameters as shown in Fig. 7, except for defining $w_0 = 0$ (Fig. 11). As the smallest patches follow a seismic cycle of $3 \times w_c = 0.3$ m and the loading rate is 0.01 m/Δt, most of smallest patches slip almost simultaneously along the fault every 30 time steps, with a visible periodicity in the total slip deficit (Fig. 11b) and seismic moment release over the fault (Fig. 11c). Since case (4) is governed by a large background area, the peaks in slip rate for the smallest patches become sparse and the slip deficit (variation in M_0) for the total system increases due to the broader background strengthening process between time steps 240 and 360. This result likely arises from the fact that the distance between two slip-weakening patches affects the interaction between them (Kaneko et al. 2010). It also implies that the background strengthening makes the interaction between patches difficult. This mechanism is unclear for case (6), because the background area is minimized for this simulation.

Finally, we change the lower limit of the patch ranks, following Ide (2014), and observe the resultant perturbations to the system behavior (Fig. 12). We simulate our 15 cases, with the same initial patch distribution as that shown in Fig. 6, but exclude the smallest patches of rank $k = 4$. The system behavior becomes simpler as the smallest patches disappear, in both the frequency and amplitude of the perturbations. Figure 13 summarizes these behaviors in terms of the local maximum and overall slip

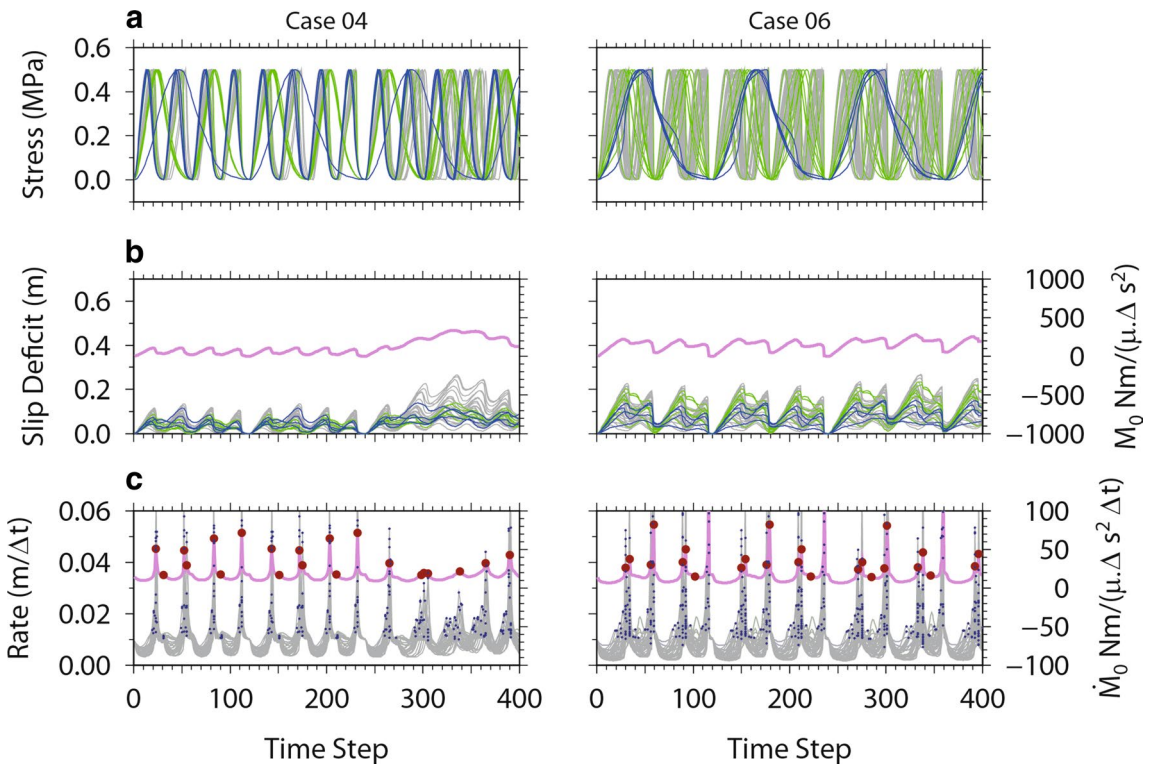

Fig. 11 Temporal evolution of the simulations for cases (4) and (6), with the same parameters settings as shown in Fig. 7, except that $w_0 = 0$. **a** Shear stress evolution at the center of each patch. The *colors* correspond to the order of patches, with *blue*, *green*, and *gray* for $k = 2, 3$, and 4, respectively. **b** Average slip deficit for each patch. M_0 is shown with a pink curve. **c** Average slip rate for each patch. $\dot{M}_0$ is shown with a *pink curve*. The local peaks of each curve are identified by red points according to the change in sign of the derivative

rates. As all the parameters are kept the same except for the existence of the small patches, a direct comparison of Fig. 13a with Fig. 8 reveals that local peaks in slip rate are mostly associated with the smallest patches in the system. The same periodic slip rate bursts exist in both cases (Figs. 8, 13), because this is governed by the larger patches that commonly exist in the system. According to the frictional state of the larger patches, the peaks in slip rate for the smallest patches may vary, as explored in the two-patch system. The relation between the peaks in slip rate is shown in Fig. 13b. Again, the overall behavior of the system (horizontal axis) does not change because it is governed by the larger patches; however, the peak value of the local slip rate is reduced because of the disappearance of the smallest patches.

In this study, we have adopted a slip-dependent friction law to characterize the variations along the fault interface that are necessary for sliding (fracture energy). As demonstrated by Noda et al. (2013), and which is also well known in the coseismic process (Bizzarri and Cocco 2003), this could be translated to a rate and state friction law (Ruina 1983). In particular, we have a priori fixed a slip cycle, but the healing process should be more complex due to the fault rheology. Nakatani (2001) argued that the state variable represents the fault strength such that its evolution obeys both slip-weakening and log-time healing. The scale of the characteristic distance in the rate- and state-dependent law also produces stable and unstable behaviors within the system (Hori and Miyazaki 2011). The advantage of the introduction of an explicit form of the slip-dependent relation, Eq. (4), is the clear definition of when the turning point in frictional behavior from strengthening to weakening occurs, such that any point on the fault interface experiences both states repeatedly. This slip dependency can provide a simpler way to describe the shallower part of the fault interface, which is largely stable during seismic cycles but sometimes becomes unstable and can potentially generate a tsunami earthquake or a mega-earthquake (e.g., Sun et al. 2017). Such a change from strengthening to weakening, or extra weakening during a mega-earthquake, can be regarded as the result of either a hydrothermal interaction during sliding (e.g., Kanamori and Heaton 2000; Noda and Lapusta 2013), the presence of weak clay minerals (Ujiie et al. 2013), or fault-related melting (Hirose and Shimamoto 2005). In our model, slip

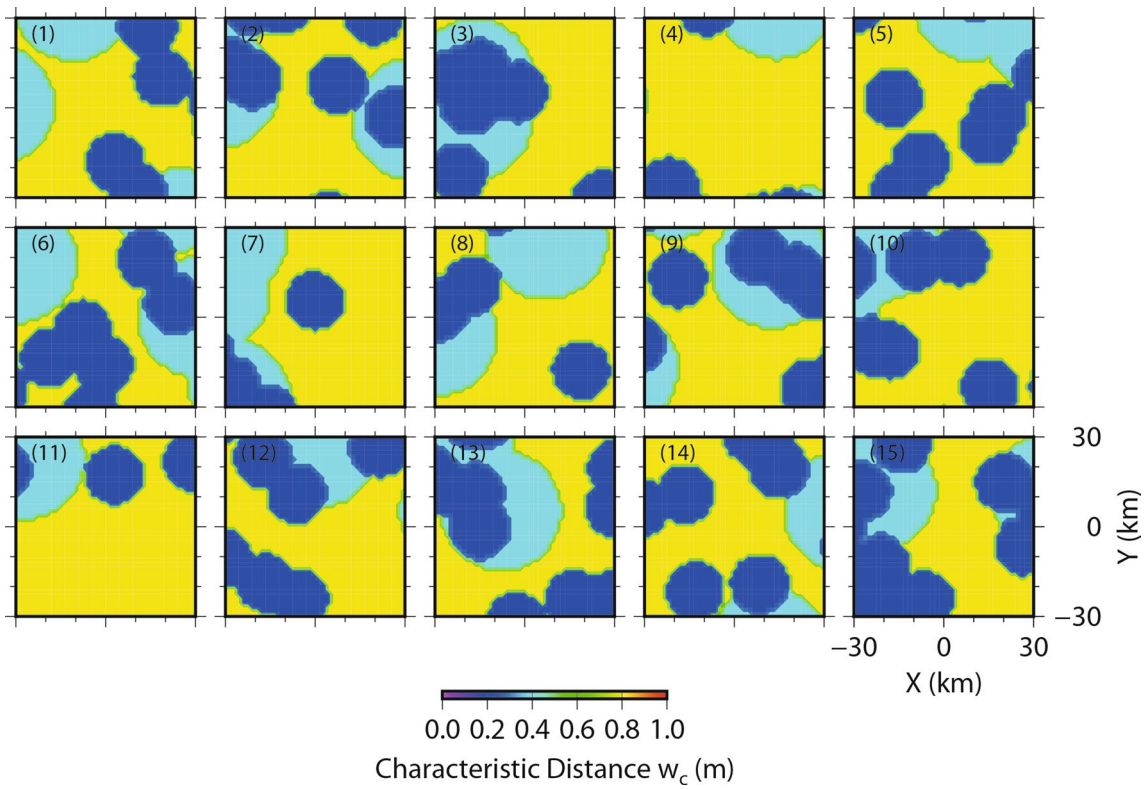

Fig. 12 Spatial distribution of multiscale patches for all 15 simulations, originating from those shown in Fig. 6. The lower limit of the structure is changed so that the smallest patches of rank $k = 4$ are removed

on small patches can be repeated very quickly once the surrounding slip is large enough. This supports the initial point of view of the multiscale concept in fracture energy (Ohnaka 2003; Ide and Aochi 2005), where the fracture energy reflects an irregular surface topography (Matsu'ura et al. 1992). Nevertheless, the rate effect or healing is oversimplified in our study, since we assume a strictly periodic behavior over slip and the same peak strength, even though the rate effect was weak during SSEs in Guerrero, Mexico (Maury et al. 2014). It is unknown whether a small heterogeneity remains in its original state after a large slip event. A more complex time-dependent process is probably required, which is also dependent on patch size (Aochi and Matsu'ura 2002).

The simulation results are informative with respect to the conceptual earthquake model. We have increased the complexity from a single patch to multiple patches and observed that the system behaviors become increasingly complex. In our numerical simulations, the peaks in slip rate from the smallest patches are the most visible, with the existence of large patches hidden in the background. Nevertheless, the frictional status of large-scale patches changes the slip rate on the small patches, such that the background strengthening process weakens the peaks in slip rate peaks on the small patches. In the case of multiscale patches, the system complexity is controlled by the lower and upper fractal limits (Ide 2014). Slip rates on the small patches become visible as tremor-like burst activity, with the amplitude and frequency of the bursts controlled by the status of the surrounding larger patches (Fig. 14). Since it is considered that a large patch evolves gradually with time (Fig. 13), the upper limit of the fractal structure evolves with time during a long seismic cycle. If a variation in slip along the fault interface (which arises from small patches) is detected, this would help us to better understand changes in the surrounding, or background, frictional status at a larger scale. Conversely, a change in this lower limit (small patches) has an immediate impact on the system behavior, as the lack of small patches leads to a repeating behavior with moderate slip rates.

The wide variety of SSEs worldwide might be explained by their differences in hierarchical structure. For example, in Guerrero, Mexico, where very large SSEs occur, it is possible that intermediate-scale patches are poorly developed. The segmentation structures of tremors observed at Nankai (Obara 2010) and Cascadia (Brudzinski and Allen 2007) may correspond to a hierarchical

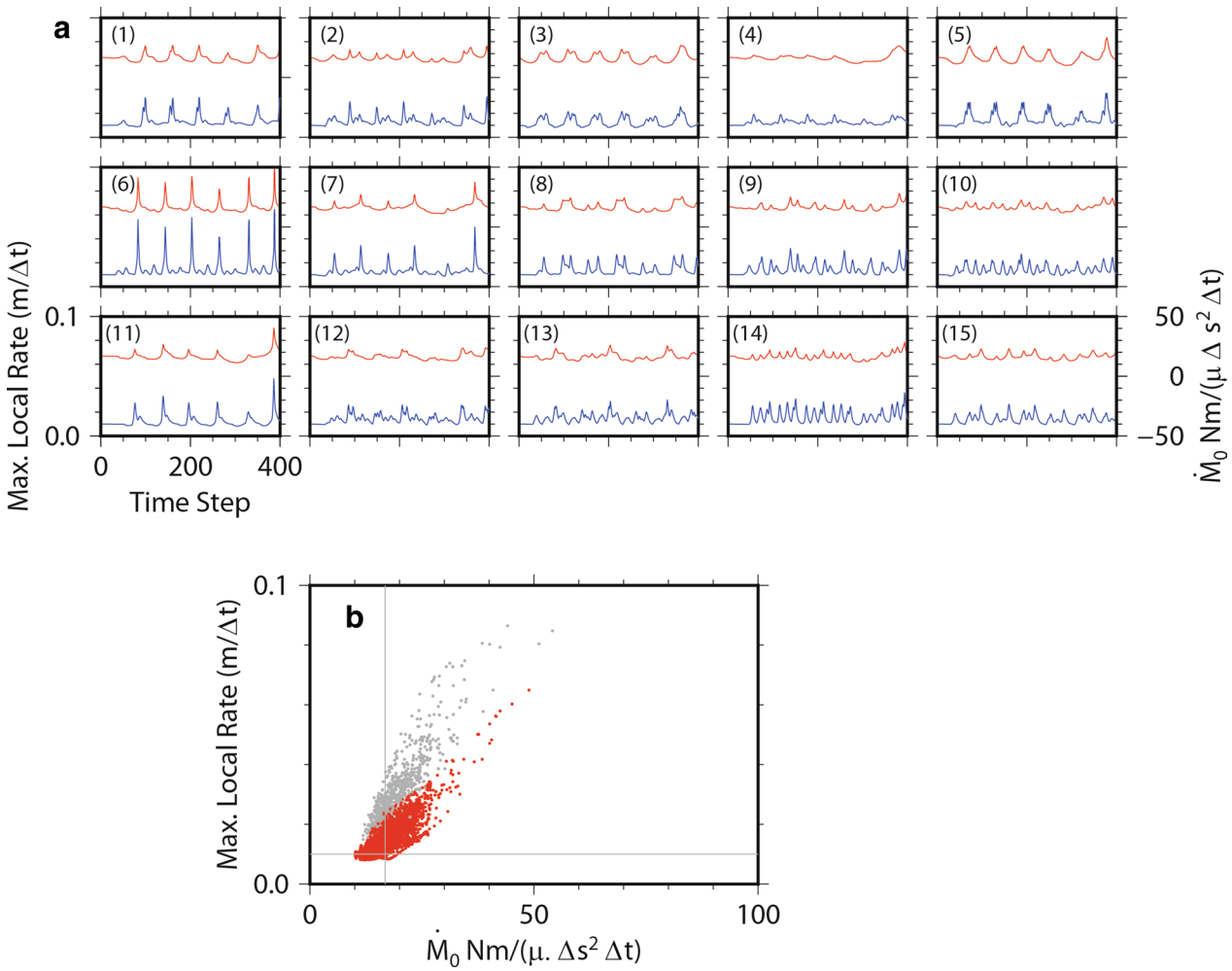

Fig. 13 Temporal evolution of all 15 simulations from Fig. 11. **a** The maximum slip rate at each time step is in *blue* (*left axis*) and the seismic moment release rate from the whole area is in *red* (*right axis*). **b** Relationship between the above two values from all 15 simulations, denoted by *red points*. *Gray points* represent the relationship for the case that includes the smallest patches $k = 4$, from Fig. 8

structure consisting of a nearly continuous distribution of many small patches along the trench, with a few very large patches controlling the recurrence intervals of tremor burst, together with some intermediate-scale patches. Conversely, in some spotty tremor regions in southwestern Japan (Ide and Tanaka 2014) and Taiwan (Ide et al. 2015), where tremors occur quasi-regularly, the interface heterogeneity is represented principally by isolated small patches.

While this study applies hierarchical structures to model stable slip along the plate interface, similar models might also be applicable to regions with small-scale unstable patches on larger-scale stable structures. One example would be eastern Japan, where many small to moderate repeating earthquakes are observed (e.g., Uchida et al. 2003). These events are usually attributed to the repeated rupture of small patches on a homogeneous and stably sliding background. There may exist a multiscale structure of stable patches behind them, but it would be difficult to observe this complex structure within the limited period of the seismic cycle (Uchida et al. 2016). Nevertheless, the long-term observation of slip-deficit evolution and differences in amplitude for repeating events may provide further insight into the complex structure of the plate interface.

Conclusions

We performed quasi-static numerical simulations of fault slip on an interface characterized by multiscale heterogeneity (patches), assuming that the characteristic distance in frictional behavior is scale-dependent. Stress accumulation on patches (e.g., strengthening process) prior to

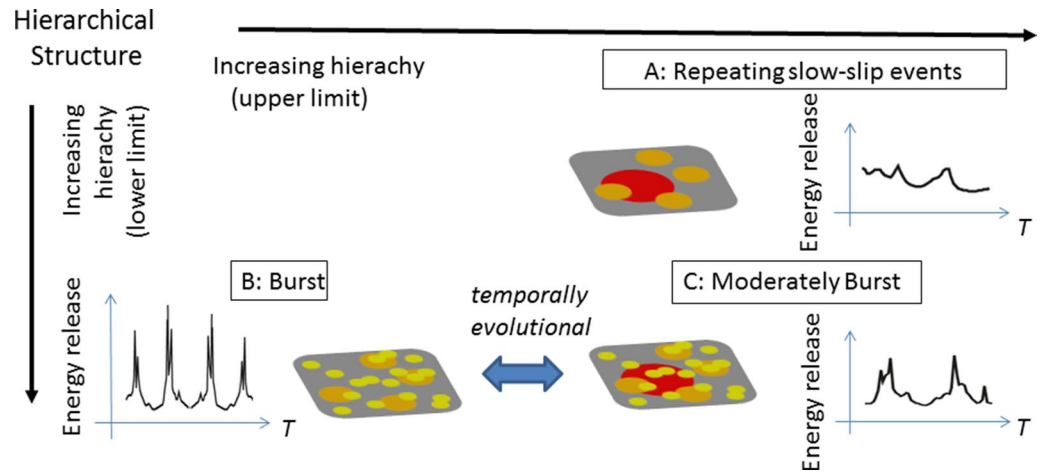

Fig. 14 Schematic illustration of fault hierarchy heterogeneity and different appearances of seismic behavior. **a** When the smallest scale is missed, the fault behavior appears as repeating slow slip events. **b** When the largest scale is missing (or there is a zero-stress background), burst seismicity controlled by small patches becomes dominant. **c** When the largest scale patch plays a strengthening role, the burst behavior is reduced

the weakening process depends on the patch size. For an isolated single patch, the evolution of slip rate is self-similar under the same loading if friction is scale-dependent, as is known for standard earthquakes. In the interaction between two patches, the behavior of a small patch can be changed by the stress condition of the surrounding region. In the case of multiscale patches, slip on small patches becomes visible, while the role of a large patch remains hidden behind. However, the frequency and maximum slip rate of slow events decrease when the surrounding region is in the strengthening regime. It is thus important to know the stress state of the large patch behind the small patches in order to describe the behavior of the whole system.

The results of this systematic study are important in improving our understanding of the heterogeneity along a fault interface for both ordinary (fast) and slow earthquakes. Since fault heterogeneity must be associated with the multiscale geometrical irregularity of the plate interface, such structures may be long-lived and remain unchanged during a few seismic cycles. These potential changes in stability may also depend on the scale of the concerned heterogeneity of the events, suggesting that there are various types of mixed behaviors associated with fast and slow slip. The slip behavior modeled in the present paper should be considered as one end-member of various slip behaviors (slow earthquakes); the other end-member (fast earthquakes) has previously been demonstrated by Aochi and Ide (2009) and related works.

Authors' contributions

HA developed the numerical codes. Both authors worked on the model conception, parameterization, simulation execution, and interpretation, and contributed to discussions and writing of the manuscript. Both authors read and approved the final manuscript.

Author details

[1] Bureau de Recherche Géologiques et Minières, 3 Avenue Claude Guillemin, BP36009, 45060 Orléans, Cedex, France. [2] Laboratoire de Géologie, Ecole Normale Supérieure/CNRS UMR 8538, PSL Research University, 24 Rue Lhomond, 75231 Paris, Cedex 5, France. [3] Research Center for Urban Safety and Security, Kobe University, Nada, Kobe 657-8501, Japan. [4] Graduate School of Science, The University of Tokyo, 1-1-1 Hongo, Bunkyo-ku, Tokyo 113-0033, Japan.

Acknowledgements

This work started in the framework of the French national project S4 (Subduction Slow and Standard Seismology; ANR-11-BS56-0017), with funding from Agence Nationale des Recherches, and then was partially supported by MEXT, Japan, under its Earthquake and Volcano Hazards Observation and Research Program, and KAKENHI (16H02219 and 16H06477).

Availability of data and materials

The simulation datasets supporting the conclusions of this article are included within the article.

Competing interests

The authors declare that they have no competing interests.

Publisher's Note

Springer Nature remains neutral with regard to jurisdictional claims in published maps and institutional affiliations.

Received: 10 January 2017 Accepted: 27 June 2017
Published online: 11 July 2017

References

Ando R, Nakata R, Hori T (2010) A slip pulse model with fault heterogeneity for low-frequency earthquakes and tremor along plate interface. Geophys Res Lett 37:L10310. doi:10.1029/2010GL043056

Ando R, Takeda N, Yamashita T (2012) Propagation dynamics of seismic and aseismic slip governed by fault heterogeneity and Newtonian rheology. J Geophys Res 117:B11308. doi:10.1029/2012JB009532

Aochi H, Fukuyama E (2002) Three-dimensional nonplanar simulation of the 1992 Landers earthquake. J Geophys Res 107(B2):2035. doi:10.1029/2000JB000061

Aochi H, Ide S (2004) Numerical Study on multi-scaling earthquake rupture. Geophys Res Lett 31:L02606. doi:10.1029/2003GL018708

Aochi H, Ide S (2009) Complexity in earthquake sequences controlled by multi-scale heterogeneity in fault fracture energy. J Geophys Res 114:B03305. doi:10.1029/2008JB006034
Aochi H, Ide S (2011) Conceptual multi-scale dynamic rupture model for the 2011 Off-the-Pacific-Coast-of-Tohoku earthquake. Earth Planets Space 63:761–765. doi:10.5047/eps.2011.05.008
Aochi H, Ide S (2014) Ground motions characterized by a multi-scale heterogeneous earthquake model. Earth Planets Space 66:42. doi:10.1186/1880-5981-66-42
Aochi H, Matsu'ura M (2002) Slip- and time-dependent fault constitutive law and its significance in earthquake generation cycles. Pageoph. 159:2029–2044
Ben-Zion Y (2012) Episodic tremor and slip on a frictional interface with critical zero weakening in elastic solid. Geophys J Int 189:1159–1168. doi:10.1111/j.1365-246X.2012.05422.x
Bizzarri A, Cocco M (2003) Slip-weakening behavior during the propagation of dynamic ruptures obeying rate- and state-dependent friction laws. J Geophys Res 108:2373. doi:10.1029/2002JB002198
Brantut N, Viesca RC (2015) Earthquake nucleation in intact or healed rocks. J Geophys Res 120:191–209. doi:10.1002/2014JB011518
Brudzinski MR, Allen RM (2007) Segmentation in episodic tremor and slip all along Cascadia. Geology 35:907–910. doi:10.1130/G23740A.1
Colella HV, Dieterich JH, Richards-Dinger K, Rubin AM (2012) Complex characteristics of slow slip event in subduction zones reproduced in multi-cycle simulations. Geophys Res Lett 39:L20312. doi:10.1029/2012GL053276
Di Carli S, François-Holden C, Peyrat S, Madariaga R (2010) Dynamic inversion of the 2000 Tottori earthquake based on elliptical subfault approximations. J Geophys Res 115:B12328. doi:10.1029/2009JB006358
Dragert H, Wang KL, James TS (2001) A silent slip event on the deeper Cascadia subduction interface. Science 292:1525–1528. doi:10.1126/science.1060152
Ellsworth WL, Beroza GC (1995) Seismic evidence for an earthquake nucleation phase. Science 268(5212):851–855
Galvez P, Ampuero JP, Dalguer LA, Somala SN, Nissen-Meyer TF (2014) Dynamic earthquake rupture modeled with an unstructured 3-D spectral element method applied to the 2011 M9 Tohoku earthquake. Geophys J Int 198:1222–1240. doi:10.1093/gji/ggu203
Gao H, Schmidt DA, Weldon RJ II (2012) Scaling relationship of source parameters for slow slip events. Bull Seism Soc Am 102:352–360. doi:10.1785/0120110096
Hashimoto C, Noda A, Sagiya T, Matsu'ura M (2009) Interplate seismogenic zones along the Kuril–Japan trench inferred from GPS data inversion. Nat Geosci 2:141–144
Hirose T, Shimamoto T (2005) Growth of molten zone as a mechanism of slip weakening of simulated faults in gabbro during frictional melting. J Geophys Res 110:B05202. doi:10.1029/2004JB003207
Hori T, Miyazaki S (2011) A possible mechanism of M 9 earthquake generation cycles in the area of repeating M 7 ~ 8 earthquakes surrounded by aseismic sliding. Earth Planets Space 63:773–777. doi:10.5047/eps.2011.06.022
Ida Y (1972) Cohesive force across the tip of a longitudinal-shear crack and Griffith's specific surface energy. J Geophys Res 77:3796–3805
Ide S (2012) Variety an spatial heterogeneity of tectonic tremor worldwide. J Geophys Res 117:B03302. doi:10.1029/2011JB008840
Ide S (2014) Modeling fast and slow earthquakes at various scales. Proc Jpn Acad Ser B 90:259–277
Ide S, Aochi H (2005) Earthquakes as multiscale dynamic ruptures with heterogeneous fracture surface energy. J Geophys Res 110:B11303. doi:10.1029/2004JB003591
Ide S, Aochi H (2013) Historical seismicity and dynamic rupture process of the 2011 Tohoku-Oki earthquake. Tectonophys 600:1–13. doi:10.1016/j.bbr.2011.03.031
Ide S, Aochi H (2014) Modeling earthquakes using fractal circular patch models with lessons from the 2011 Tohoku-Oki earthquake. J Disaster Res 9(3):264–271
Ide S, Beroza GC (2001) Does apparent stress vary with earthquake size? Geophys Res Lett 28:3349–3352. doi:10.1029/2001GL013106
Ide S, Takeo M (1997) Determination of constitutive relations of fault slip based on seismic wave analysis. J Geophys Res 102:27379–27391
Ide S, Tanaka Y (2014) Controls on plate motion by oscillating tidal stress: evidence from deep tremors in western Japan. Geophys Res Lett 41:3842–3850. doi:10.1002/2014GL060035
Ide S, Beroza GC, Shelly DR, Uchide T (2007a) A scaling law for slow earthquakes. Nature 447:76–79. doi:10.1038/nature05780
Ide S, Shelly DR, Beroza GC (2007b) Mechanism of deep low frequency earthquakes: further evidence that deep non-volcanic tremor is generated by shear slip on the plate interface. Geophys Res Lett 34:L03308. doi:10.1029/2006GL028890
Ide S, Imanishi K, Yoshida Y, Beroza GC, Shelly DR (2008) Bridging the gap between seismically and geodetically detected slow earthquakes. Geophys Res Lett 35:L10305. doi:10.1029/2008GL034014
Ide S, Yabe S, Tai HJu, Chen KH (2015) Thrust type-focal mechanisms of tectonic tremors in Taiwan: evidence of subduction. Geophys Res Lett 42:3248–3256. doi:10.1002/2015GL063794
Ito Y, Obara K, Shiomi K, Sekine S, Hirose H (2007) Slow earthquakes coincident with episodic tremors and slow slip events. Science 315:503–506. doi:10.1126/science.1134454
Kanamori H, Anderson D (1975) Theoretical basis of some empirical relations in seismology. Bull Seism Soc Am 65:1073–1095
Kanamori H, Heaton TH (2000) Microscopic and macroscopic physics of earthquakes. Geophys Monogr AGU 120:147–164
Kaneko Y, Avouac J-P, Lapusta N (2010) Towards inferring earthquake patterns from geodetic observations of interseismic coupling. Nature Geosci 3:363–369. doi:10.1038/ngeo843
Kostoglodov V, Singh SK, Santiago JA, Franco SI, Larson KM, Lowry AR, Bilham R (2003) A large silent earthquake in the Guerrero seismic gap, Mexico. Geophys Res Lett 30:1807. doi:10.1029/2003GL017219
Lay T, Kanamori H, Ammon CJ, Koper KD, Hutko AR, Ye L, Yue H, Rushing TM (2012) Depth-varying rupture properties o subduction zone megathrust faults. J Geophys Res 117:B04311. doi:10.1029/2011JB009133
Linde AT, Gladwin MT, Johnston MJS, Gwyther RL, Bilham RG (1996) A slow earthquake sequence on the San Andreas fault. Nature 383:65–68. doi:10.1038/383065a0
Liu Y, Rice JR (2005) Aseismic slip transients emerge spontaneously in three-dimensional rate and state modeling of subduction earthquake sequences. J Geophys Res 110:B08307. doi:10.1029/2004JB003424
Matsu'ura M, Kataoka M, Shibazaki B (1992) Slip-dependent friction law and nucleation processes in earthquake rupture. Tectonophys 211:135–148
Maury J, Aochi H, Radiguet M (2014) Fault constitutive relations inferred from the 2009–2010 slow slip event in Guerrero, Mexico. Geophys Res Lett 41:4929–4936. doi:10.1002/2014GL060691
Mikumo T, Olsen KB, Fukuyama E, Yagi Y (2003) Stress breakdown time and slip-weakening distance from slip-velocity functions on earthquake faults. Bull Seism Soc Am 93:264–282
Nakatani M (2001) Conceptual and physical clarification of rate and state friction: frictional sliding as a thermally activated rheology. J Geophys Res 106:13347–13380
Noda H, Lapusta N (2013) Stable creeping fault segments can become destructive as a result of dynamic weakening. Nature 493:518–521. doi:10.1038/nature11703
Noda H, Nakatani M, Hori T (2013) Large nucleation before large earthquakes is sometimes skip due to cascade-up—implication for a rate and state simulation of faults with hierarchical asperities. J Geophys Res 118:2924–2952. doi:10.1002/jgrb.50211
Obara K (2002) Nonvolcanic deep tremor associated with subduction in southwest Japan. Science 296:1679–1681
Obara K (2010) Phenomenology of deep slow earthquake family in southwest Japan: spatiotemporal characteristics and segmentation. J Geophys Res 115:B00A25. doi:10.1029/2008JB006048
Ohnaka M (2003) A constitutive scaling law and a unified comprehension for frictional slip failure, shear fracture of intact rock, and earthquake rupture. J Geophys Res 108(B2):2080. doi:10.1029/2000JB000123
Ohnaka M, Yamashita T (1989) A cohesive zone model for dynamic shear faulting based on experimentally inferred constitutive relation and strong motion source parameters. J Geophys Res 94:4089–4104
Olsen KB, Madariaga R, Archuleta RJ (1997) Three-dimensional dynamic simulation of the 1992 Landers earthquake. Science 278:834–838
Palmer AC, Rice JR (1973) The growth of slip surface in the progressive failure of over-consolidated clay. Proc R Soc Lond Ser A 332:527–548
Peyrat S, Olsen KB, Madariaga R (2004) Which dynamic parameters can be estimated from strong ground motion? Pageoph 161:2155–2169
Press WH, Teukolsky SA, Vetterling WT, Flannery BP (1992) Numerical Recipes in Fortran: the art of scientific computing, 2nd edn. Cambridge University Press, Cambridge

Rohmer J, Aochi H (2015) Impact of channel-like erosion patterns on the frequency-magnitude distribution of earthquakes. Geophys J Int 202(1):670–677. doi:10.1093/gji/ggv181

Ruina AL (1983) Slip instability and state variable friction laws. J Geophys Res 88:10359–10370

Ruiz S, Madariaga R (2011) Determination of the friction law parameters of the Mw6.7 Michilla earthquake in northern Chile by dynamic inversion. Geophys Res Lett 38:L09317. doi:10.1029/2011GL047147

Shibazaki B, Iio Y (2003) On the physical mechanism of silent slip events along the deeper part of the seismogenic zone. Geophys Res Lett 30:1489. doi:10.1029/2003GL017047

Shibazaki B, Matsu'ura M (1995) Foreshocks and pre-events associated with the nucleation of large earthquakes. Geophys Res Lett 22:1305–1308

Sun T, Wang K, Fujiwara T, Kodaira S, He J (2017) Large fault slip peaking at trench in the 2011 Tohoku-oki earthquake. Nature Commun 8:14044. doi:10.1038/ncomms14044

Tada T, Fukuyama E, Madariaga R (2000) Non-hypersingular boundary integral equations for 3-D non-planar crack dynamics. Comput Mech 25(6):613–626. doi:10.1007/s004660050508

Uchida N, Matsuzawa T, Igarashi T, Hasegawa A (2003) Interplate quasi-static slip off Sanriku, NE Japan, estimated from repeating earthquakes. Geophys Res Lett 30(15):1801. doi:10.1029/2003GL017452

Uchida N, Iinuma T, Nadeau RM, Bürgmann R, Hino R (2016) Periodic slow slip triggers megathrust zone earthquakes in northeastern Japan. Science 351:488–492. doi:10.1126/science.aad3108

Uchide T, Ide S (2010) Scaling of earthquake rupture growth in the Parkfield area: self-similar growth and suppression by the finite seismogenic layer. J Geophys Res 115:B11302. doi:10.1029/2009JB007122

Ujiie K, Tanaka H, Saito T, Tsutsumi A, Mori JJ, Makeda J, Brodsky EE, Chester FM, Eguchi M, Toczko S, Expedition 343 and 343T Scientists (2013) Low coseismic shear stress on the Tohoku-oki Megathrust determined from laboratory experiments. Science 343:1211–1214. doi:10.1126/science.1243485

Zigone D, Ben-Zion Y, Campillo M (2015) Modelling non-volcanic tremor, slow slip events and large earthquakes in the Guerrero subduction zone (Mexico) with space-variable frictional weakening and creep. Geophys J Int 202:653–669. doi:10.1093/gji/ggv174

Submit your manuscript to a SpringerOpen journal and benefit from:

- ► Convenient online submission
- ► Rigorous peer review
- ► Open access: articles freely available online
- ► High visibility within the field
- ► Retaining the copyright to your article

Submit your next manuscript at ► springeropen.com